Instability of quadratic band crossing systems to topological Anderson insulating phases

Nicolau Sobrosa,[1] Miguel Gonçalves,[2] and Eduardo V. Castro[1,3]
[1]*Centro de Física das Universidades do Minho e Porto, Departamento de Física e Astronomia, Faculdade de Ciências, Universidade do Porto, 4169-007 Porto, Portugal*
[2]*CeFEMA, Instituto Superior Técnico, Universidade de Lisboa, Avenida Rovisco Pais, 1049-001 Lisboa, Portugal*
[3]*Beijing Computational Science Research Center, Beijing 100084, China*

(Received 24 January 2024; revised 12 April 2024; accepted 30 April 2024; published 10 May 2024)

Here we study the instabilities of a quadratic band crossing system to Chern insulating states and uncorrelated disorder. We determine the phase diagram in the plane of topological mass versus disorder strength, characterizing the system with respect to the spectral, localization, and topological properties. In the clean limit, the system has two gapped Chern insulating phases with Chern numbers $C = \pm 2$ and a trivial phase with $C = 0$. For finite disorder, the quadratic band crossing points are unstable to emergent gapless Chern insulating phases with $C = \pm 1$ that are not present in the clean limit. These phases occupy a considerable region of the phase diagram for intermediate disorder and show features of topological Anderson insulators: it is possible to reach them through disorder-driven transitions from trivial phases.

DOI: 10.1103/PhysRevB.109.184206

I. INTRODUCTION

Topological insulators are a remarkable state of electronic matter. They show quantized responses that are proportional to topological invariants and, as a consequence, are typically very robust to perturbations and system details [1–4]. Topological band insulators, as paradigmatic examples of systems with nontrivial topology, have been extensively studied and are fairly well understood [3]. Nontrivial topology, however, also manifests in systems with broken translational invariance that are not described by topological band theory. Among these systems, disordered topological insulators are a popular subgroup [5].

Topological phases are robust to disorder in that no symmetry protecting the topological properties is broken [6,7]. In quantum Hall insulators, disorder even plays a fundamental role in the observation of a quantized Hall conductance. More generally, it is now well established that in the case of Chern insulators, where time-reversal symmetry is broken, uncorrelated disorder localizes every eigenstate except at specific energies [8–12]. The extended eigenstates at these energies carry finite Chern numbers and are therefore responsible for a quantized Hall response as long as the Fermi level lies between them (the localized states cannot change this response). Topological phase transitions in disordered Chern insulators occur when the extended states merge and annihilate at the Fermi level (through the so-called levitation and annihilation mechanism), becoming localized [10].

The localization properties of noninteracting topological systems can be understood within a low-energy description in terms of random, massive Dirac Hamiltonians [13]. Generic phase diagrams in the plane of Dirac mass versus disorder strength have been obtained for all 10 symmetry classes from the tenfold way [14]. For class A, to which Chern insulators belong, the phase diagram consists of multiple localized phases which can be distinguished by their Chern number and are separated by phase boundaries at which the localization length diverges. However, not all Chern insulators can be derived from massive Dirac Hamiltonians at low energies. A well-known example is quadratic band crossing (QBC) systems.

Systems with quadratic band crossings in two dimensions are very interesting because, contrary to conventional band degeneracy points, they are associated with a finite Berry phase of $\pm 2\pi$. Due to the finite density of states at the QBC, these systems are unstable to interactions [15], leading to nematic phases with two Dirac cones, each carrying half of the QBC's Berry phase, or gap openings that may give rise to topological insulating phases precisely due to the nontrivial Berry phase of the QBC [16–19]. The fate of interaction-induced topological insulating phases in the presence of disorder was examined in Refs. [20,21] within the one-loop Renormalization Group (RG) approach. The suppression of topological phases under increasing disorder and a possible transition to trivial phases were predicted.

Quite surprisingly, there are systems which show topological phase transitions from trivial to topological phases with increasing disorder. This disorder-driven topological phase is now known as a topological Anderson insulator (TAI) [22,23]. This phase has been observed in many models, including paradigmatic models of topological insulators in two dimensions such as the Kane-Mele model [24,25] and the disordered Haldane model [26–28], in the one-dimensional Su Schrieffer Heeger (SSH) model [29], in quasiperiodic systems [30,31], and, more recently, in non-Hermitian models [32]. Whether TAI phases may be realized for Chern insulators derived from QBC systems is still an open question. Moreover, the fate of the QBC itself in the presence of disorder has received little attention.

In this work we study the interplay between the instability of a two-dimensional (2D) QBC system to a Chern

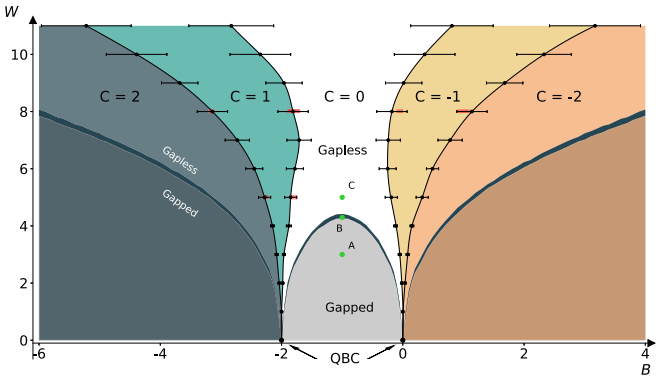

FIG. 1. Phase diagram in the B-W plane. The Chern number was calculated for a system with 35×35 lattice points and was averaged over 100 disorder realizations. The gray areas, below the thicker lines, correspond to the gapped regions obtained through calculations of the DOS. The error bars for the Chern number were obtaining by fixing the disorder intensity and varying B. The red boxes indicate the results for the critical points calculated with the TMM. The size of the bar is determined in such a way that outside the bar the system is clearly localized (Λ_M decreases with M; see Fig. 5 and the text).

insulating state and disorder of the Anderson type. The full phase diagram in the plane of the gap opening coupling parameter B and disorder strength W is shown in Fig. 1. For null disorder, QBC points (QBCPs) occur for $B = -2, 0$, while the system is a gapped trivial insulator or a Chern insulator with Chern number $C = \pm 2$ for any other B value. These phases are also present for finite disorder, but new gapless Chern insulating phases also emerge. Besides gapless and gapped phases with $C = \pm 2$, new gapless topological phases with $C = \pm 1$ not present in the clean limit arise. In fact, the most important result of our work is that the QBCPs are unstable to the formation of these phases for any finite disorder. Finally, the existence of TAI phenomena is also clear: it is possible to cause a transition between the trivial phase and the disorder-induced topological phases with $C = \pm 1$ by increasing disorder.

This paper is organized as follows: In Sec. II, we introduce the tight-binding model used to describe the electronic properties of the disordered QBC system and the methods to analyze its properties. The topological, spectral, and localization properties are discussed in Sec. III. A thorough discussion of the obtained results is given in Sec. IV. In Sec. V the key results are summarized, and some conclusions are drawn. We also include six Appendixes: in Appendix A we present the real-space tight-binding Hamiltonian and a schematic representation; in Appendix B we show edge states inside the gap for open boundary conditions. In Appendix C we provide the phase diagram for binary disorder; in Appendix D we discuss the criterion used to distinguish gapped and gapless regimes. An example of a possible $\mathbf{k}$-dependent self-energy that would lead to a $C = 1$ phase in the self-consistent Born approximation is given in Appendix E; the robustness of the obtained phase diagram when the QBC is split into two Dirac cones is discussed in Appendix F.

II. MODEL AND METHODS

We study a QBC system realized on a square lattice with two orbitals per site. The model considers first-neighbor hoppings between the same orbitals and second-neighbor hoppings coupling different orbitals. The Hamiltonian for the disorder-free model can be written in reciprocal space as

$$H_0 = \sum_{\mathbf{k}} \Psi_{\mathbf{k}}^{\dagger} \mathcal{H}_{\mathbf{k}} \Psi_{\mathbf{k}}, \tag{1}$$

where $\Psi_{\mathbf{k}}^{\dagger} = (c_{\mathbf{k}1}^{\dagger}, c_{\mathbf{k}2}^{\dagger})$ is the two-component spinor in the space of the two orbitals, where $c_{\mathbf{k}\alpha}$ creates an electron with Bloch momentum $\mathbf{k}$ in orbital α, and

$$\mathcal{H}_{\mathbf{k}} = \mathbf{h} \cdot \boldsymbol{\sigma}, \tag{2}$$

with $\boldsymbol{\sigma}$ being the Pauli vector and $\mathbf{h}$ being the vector given by

$$\begin{aligned} h_x &= 2t_x \sin k_x \sin k_y, \\ h_y &= 0, \\ h_z &= 2t_z(\cos k_x - \cos k_y). \end{aligned} \tag{3}$$

In the following, we set $t_x = t_z = t$ and t to unity.

This model has two QBCPs at $\Gamma = (0, 0)$ and $M = (\pm\pi, \pm\pi)$. By adding a finite h_y, it is possible to open a gap. For a constant h_y, the system is a trivial insulator. Like in the Haldane model [33], we may add a k-dependent component which allows us to tune independently the gap at each QBCP. In the following we use a simple choice which depends on a single parameter, B:

$$h_y = 1 + \frac{B+1}{2}(\cos k_x + \cos k_y). \tag{4}$$

This type of k dependence implies the breaking of time-reversal symmetry since, as seen from Eq. (2), we have $\mathcal{H}_k \neq \mathcal{H}_{-k}^{*}$. As shown below, the system will become a Chern insulator for some intervals of B values.

In real space, the constant term corresponds to an intracell complex hopping between different orbitals, and the term with k modulation corresponds to a nearest-neighbor complex hopping between different orbitals. As the modification in Eq. (4) does not change h_x and h_z, a QBCP still exists when $h_y = 0$, as seen before. For $B = 0$, there is a QBCP at M, and for $B = -2$, there is a QBCP at Γ.

Adding the disorder potential, the Hamiltonian reads

$$H = H_0 + \sum_i \sum_{\alpha=1,2} \xi_{i\alpha} \hat{c}_{i\alpha}^{\dagger} \hat{c}_{i\alpha}, \tag{5}$$

where $\xi_{i\alpha}$ are site-dependent potentials that follow the uniform distribution (Anderson disorder),

$$P_W(\xi_{i\alpha}) = \frac{1}{W} \Theta\left(|\xi_{i\alpha}| - \frac{W}{2} \right), \tag{6}$$

where W defines the disorder strength. Note that H_0 in Eq. (5) is the Hamiltonian in Eq. (1) written in the real-space basis. The details are presented in Appendix A, where a sketch of the hoppings is also shown. In Appendix C we present the phase diagram obtained for the case of binary disorder. The result is very similar to that in Fig. 1 obtained for Anderson disorder, and the conclusions are qualitatively the same.

We carried out a complete study of the phase diagram of the model in Eq. (5), characterizing the spectral, topological, and localization properties. The density of states (DOS) was calculated for finite systems containing more than 10^6 sites using the KITE [34] quantum transport software, which has a very efficient implementation of the kernel polynomial method (KPM).

The topological phase diagram was obtained by computing the Chern number using the coupling matrix method introduced in Refs. [35,36]. This method allows the computation of the Chern number with a single exact diagonalization of a system with periodic boundary conditions. Considering a 2D lattice with $N = L_x \times L_y$ unit cells, for a particular disorder configuration, with eigenvectors denoted by $|\psi_n(\boldsymbol{r}_i)\rangle$, the coupling matrices are defined by

$$C^{mn}_{\boldsymbol{q},\boldsymbol{q}'} = \langle \psi_m \mid e^{i(\boldsymbol{q}-\boldsymbol{q}')\cdot \boldsymbol{r}_i} \mid \psi_n \rangle$$

for a given pair of momenta $\boldsymbol{q}$ and $\boldsymbol{q}'$. For big enough system sizes ($L_{x/y} \gtrsim 15$), it is enough to consider the following set of momenta: $\{\boldsymbol{q}_0 = (0,0), \boldsymbol{q}_1 = (\frac{2\pi}{L_x}, 0), \boldsymbol{q}_2 = (\frac{2\pi}{L_x}, \frac{2\pi}{L_y}), \boldsymbol{q}_3 = (0, \frac{2\pi}{L_y})\}$. By constructing the matrix

$$\mathcal{F} = C_{\boldsymbol{q}_0\boldsymbol{q}_1} C_{\boldsymbol{q}_1\boldsymbol{q}_2} C_{\boldsymbol{q}_2\boldsymbol{q}_3} C_{\boldsymbol{q}_3\boldsymbol{q}_0}, \tag{7}$$

the Chern number is obtained through the eigenvalues $\{\lambda_p\}$ of Eq. (7),

$$C = -\frac{1}{2\pi} \sum_p \arg \lambda_p. \tag{8}$$

We note that, even though the Chern number computed for each disorder realization is an integer within numerical accuracy, the averaged Chern number may change continuously and present nonquantized values due to finite size effects.

The localization properties were characterized through the transfer matrix method (TMM) [37–39], which also allowed us to cross-check the Chern number results. This method considers a finite system with a large longitudinal length L and a transverse width M which we varied in order to find the localization length for a given M, λ_M. Considering this setup, we may write the Hamiltonian in a generic manner as

$$H = \sum_n \sum_{ij} |n,i\rangle \epsilon_n^{ij} \langle n,j| \tag{9}$$

$$+ |n+1,i\rangle V^{ij}_{n+1,n} \langle n,j| + |n,i\rangle V^{ij}_{n,n+1} \langle n+1,j|. \tag{10}$$

The state $|n,i\rangle$ corresponds to an orbital at site i of the nth transverse slice. The parameters ϵ_n^{ij} correspond to the disorder and hoppings in the same slice, and $V_{n+1,n}$ or $V_{n,n+1}$ connects adjacent slices. For a given state $|\Psi\rangle = \sum_{n,i} A_n^i |n,i\rangle$, we can write the Schrödinger equation for a specific energy E as

$$\begin{pmatrix} \boldsymbol{A}_{n+1} \\ \boldsymbol{A}_n \end{pmatrix} = \boldsymbol{M}_n \begin{pmatrix} \boldsymbol{A}_n \\ \boldsymbol{A}_{n-1} \end{pmatrix}, \tag{11}$$

where $\boldsymbol{M}_n$ defines the transfer matrix. Defining the cumulative transfer matrix $\boldsymbol{T}_N = \prod_{n=0}^{N} \boldsymbol{M}_n$, we are able to extract the localization length λ_M through its eigenvalues. The localization properties may then be inferred from the normalized localization length $\Lambda_M = \lambda_M/M$ in the following way: if Λ_M decreases with M, the states are localized in the thermodynamic limit, which corresponds to an insulating behavior; on the other hand, if Λ_M increases with M, the states are extended. A constant Λ_M is characteristic of critical states that appear at transition points between different phases. We choose L so that λ_M is calculated with an error less than 1%. We note that the behavior of Λ_M can capture topological phase transitions at finite disorder. As mentioned in the Introduction, the spectrum of finite-disorder Chern insulators consists of localized states, except at specific energies where critical states live. Topological phase transitions occur when these states cross (and merge at) the Fermi level. Therefore, for a disordered Chern insulator, Λ_M should always decrease with M except at the topological phase transitions, where it becomes M independent.

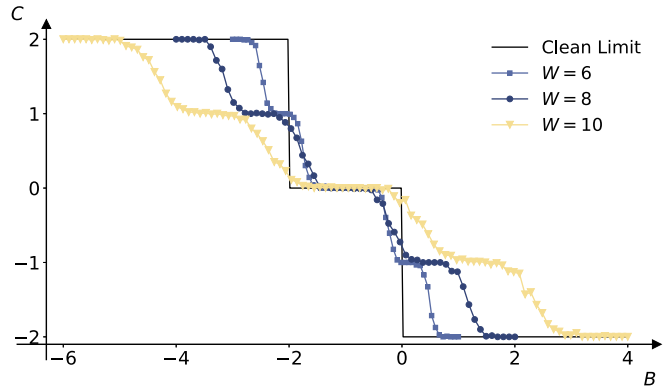

FIG. 2. Chern number results obtained at fixed W and variable B. The results were averaged over 120 disorder realizations. Each color depicts three examples of the disorder intensities used. The solid black curve represents the topological phases of the system calculated for null disorder where it is clear that no $C = \pm 1$ phases exist.

III. RESULTS

A. Topological properties

In this section we present details of the topological phase diagram in Fig. 1. The different colors indicate different Chern numbers, and the black thin lines represent the topological transitions. For null disorder the system undergoes a transition from $C = \pm 2$ to $C = 0$ at the points where a QBCP appears, that is, for $B = -2$ and $B = 0$. For finite disorder, the phases with $C = 0, \pm 2$ survive, and new gapless phases with $C = \pm 1$ appear. The latter phases are TAIs as it is possible to reach them by increasing disorder from a topologically trivial phase at fixed B. For large enough disorder, all topological phases are suppressed, in agreement with one-loop RG calculations [20] for interacting QBC systems.

To obtain the transition lines, the disorder strength W was fixed at some value, and the gap opening parameter B was varied continuously. For each disorder strength we performed an average over 120 different disorder configurations in a lattice with 35×35 sites. Some examples of the obtained curves are represented in Fig. 2, including the values for the clean limit. The continuous variation of the averaged Chern number is expected to disappear in the thermodynamic limit, where transitions between different Chern numbers should become sharp. The error bars that appear in Fig. 1 are determined

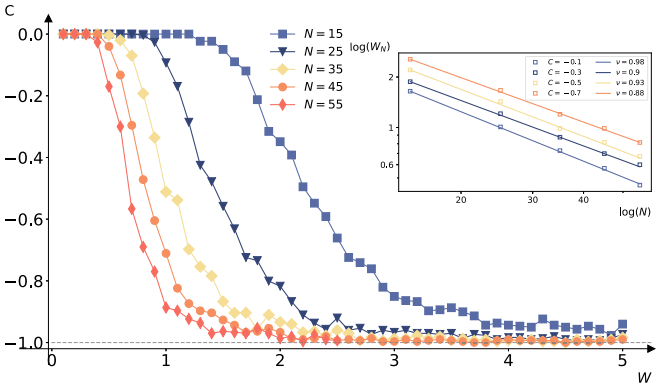

FIG. 3. Chern number averaged over 300 disorder realizations as a function of disorder strength W for $B = 0$ (QBC at $W = 0$) and variable system sizes containing $N \times N$ sites. Inset: Scaling of some fixed Chern numbers as a function of the number of sites. ν indicates the scaling as $N^{-\nu}$.

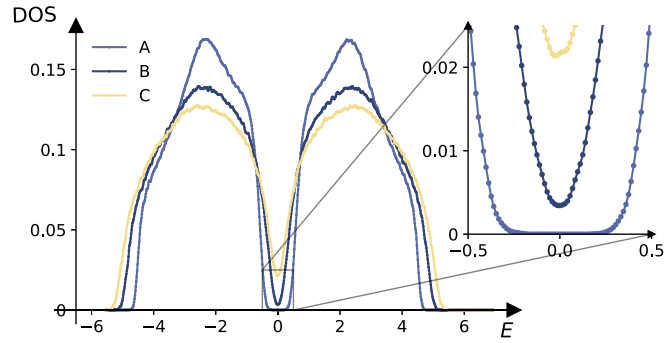

FIG. 4. Examples of the DOS calculated for points A, B, and C marked in Fig. 1. The inset shows a zoom around the Fermi level which corresponds to $E = 0$ at half filling. An average over 20 disorder realizations was performed, and a system of 1024×1024 sites was considered.

through an analysis of curves like the ones shown in Fig. 2: the length of the bar indicates the range over which the Chern number was more than 5% away from its integer value.

From the phase diagram in Fig. 1, it is not clear whether finite-disorder Chern insulating phases with $C = \pm 1$ exist for any infinitesimal disorder. In order to shed light on whether this is the case, we fixed $B = 0$ (QBC system in the clean limit) and computed the Chern number as a function of W for different system sizes. The results are shown in Fig. 3, where it is clear that the $C = -1$ phase occurs for disorder strengths that approach $W = 0$ as the system size is increased. In the inset of Fig. 3 we plot, for fixed C values in the apparent transition region, the corresponding disorder strength W_N for each size N. The fits clearly indicate that the transition should occur discontinuously at $W = 0$ in the thermodynamic limit. Although we are limited numerically from reaching larger system sizes, these results support the conjecture that in the thermodynamic limit the $B = 0$ QBCP is unstable to the formation of the $C = -1$ phase for any infinitesimal disorder. The same is expected for the QBCP at $B = -2$, as suggested by the symmetry of the phase diagram around $B = -1$.

B. Gapped and gapless regions

In order to study the existence of a spectral gap at the Fermi level ($E = 0$ at half filling) we computed the DOS using the KPM as implemented in KITE [34]. In Fig. 1 we present the gapped-gapless transitions with thicker lines and shaded gapped regions in gray. Examples of the DOS are shown in Fig. 4 for systems with parameters corresponding to the points marked A, B, and C in the phase diagram in Fig. 1. As seen in the inset, system A is clearly gapped, with zero DOS at and around $E = 0$. System C is gapless, as it presents a finite DOS at and around $E = 0$. Although system B also presents a finite DOS, its value at $E = 0$ is small. In such cases, we used a criterion to distinguish gapless from gapped systems, as explained next.

The system was considered gapped when the DOS at the Fermi level was below a certain threshold ρ_{cut} that was determined by exact diagonalization of the Hamiltonian in Eq. (5). In Appendix D we detail the analysis we performed and show results that support our choice. The error in the transition from gapped to gapless regions corresponds to a variation of $\pm 25\%$ of ρ_{cut}. This error corresponds to the thickness of the gapped-gapless transition lines in Fig. 1. The small error shows that variations in the criterion do not significantly affect the results, especially in the regions of the topological phase transitions.

C. Localization properties

We studied the normalized localization length Λ_M obtained with the TMM at the Fermi level ($E = 0$). We recall that in Chern insulating systems, we expect Λ_M to always decrease with M, except at specific points. This means that, as expected, all states at the Fermi level are localized except when a topological phase transition occurs and is accompanied by the merging of critical states carrying opposite Chern numbers. Example results are shown in Fig. 5. The results in Fig. 5(a) are for $W = 5$ and a range of B containing the $C = 2$ to $C = 1$ and $C = 1$ to $C = 0$ transitions. Figure 5(b) corresponds to a cut at $W = 8$ for a range of B containing all the topological phase transitions in the system. The phase transition points were considered to be those with constant Λ_M. The uncertainty in these points was considered to be the range of B over which there is no clear decrease in Λ_M with M. This uncertainty is represented in Fig. 1 by the shaded red bars and is perfectly bounded by the error bars in the Chern number.

IV. DISCUSSION

The phase diagram of the QBC system unveiled here shows many features that are characteristic of well-known disordered topological insulators [9–12,22,23,25–28,40–46], such as the existence of robust finite-disorder gapped and gapless topological insulating phases. However, there is a feature that distinguishes it from previously explored models: the existence of new disorder-driven topological phases with $C = \pm 1$ absent in the clean limit.

Particularly interesting are the plateau transitions $C = \pm 2 \to \pm 1 \to 0$ at finite disorder strength as the topological gap parameter B is changed, as shown in Fig. 2. This shows

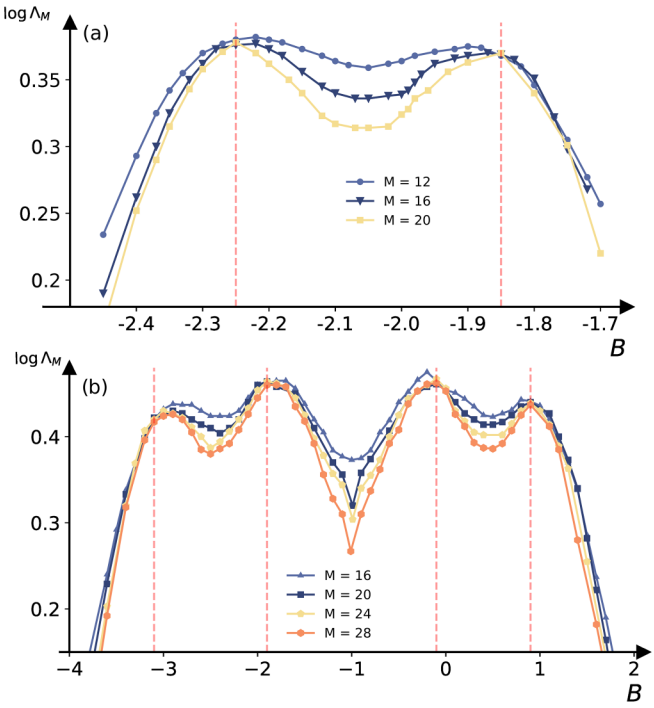

FIG. 5. Normalized localization length Λ_M as a function of the gap opening parameter B for systems with varying width M and (a) disorder $W = 5$ and (b) $W = 8$. The vertical dashed lines indicate the critical points.

that an equivalent plateau sequence is possible with increasing disorder. This possibility is conjectured to be ruled out in quantum Hall systems [47] and other Chern insulators derived from Dirac (linear band crossings) Hamiltonians [48]. In those systems, starting with $|C| \geqslant 2$, the plateau transition $\Delta C = \pm 1$ is never observed with increasing disorder due to ensemble averaging over disorder realizations.

Our results suggest that the existence of a QBCP is a key ingredient for the formation of these phases. In particular, the finite-size scaling analysis in Fig. 3 is a strong indication that they are instabilities of the QBCPs: in the thermodynamic limit, any infinitesimal amount of disorder should drive the QBC system to one of these phases. Furthermore, from the phase diagram in Fig. 1, it is clear that for low disorder the new topological phases are located around the clean-limit QBCP.

The new phases with $C = \pm 1$ are also TAIs since they can be reached by increasing disorder from a trivial phase. TAI phenomena have been observed in a multitude of disordered topological insulators. However, there is an important difference from the conventional TAI in the present case: the $C = \pm 1$ TAI phases have a Chern number that does not exist in any zero-disorder topological phase of the model. Therefore, these TAI phases do not evolve smoothly from the clean-limit phases as disorder is increased, in contrast to conventional TAIs.

For conventional TAIs, a self-consistent, low-order Born approximation is usually enough to capture the topological phase transition [23,49]. In the present case, since the $C = \pm 1$ phases are not present at zero disorder, a perturbative approach is not well justified. Moreover, within the Born approximation a k-independent self-energy is obtained, which translates into a renormalization of the parameters of the original model. For the Hamiltonian in Eq. (2), no k-independent self-energy of the general form $\Sigma = \mathbf{\Sigma} \cdot \boldsymbol{\sigma}$, with $\mathbf{\Sigma} = (\Sigma_x, \Sigma_y, \Sigma_z)$, is able to induce a $C = \pm 1$ phase. Nevertheless, a k-dependent translationally invariant perturbation $\Sigma(\mathbf{k}) = \mathbf{\Sigma}(\mathbf{k}) \cdot \boldsymbol{\sigma}$ may give rise to the $C = \pm 1$ phase, as shown in Appendix E for a particular example with $\mathbf{\Sigma}(\mathbf{k}) = (\Sigma_x(\mathbf{k}), 0, 0)$. In Appendix E we even show that the clean-limit model with the proposed k-dependent perturbation is adiabatically connected to the disorder-induced $C = \pm 1$ TAI we found for our QBC system. However, for the uncorrelated disorder used here, no k-dependent self-energy is allowed, which invalidates such an approach.

A possible variation of the QBC system is to split the QBCP into two Dirac cones with a suitable perturbation (see Appendix F). Even in this case, finite disorder gives rise to the $C = \pm 1$ phases, which could be an argument against the importance of the QBCP for their existence. Nonetheless, the topological information carried by the split Dirac cones and the QBCP is the same since no gap is opened in the splitting process. The topological properties of the new system can then be traced back to the possibility of creating a QBCP without closing the gap.

Finally, the results obtained here are not restricted to disorder of the Anderson type. We also obtained the phase diagram for binary disorder, which is qualitatively similar to the phase diagram for Anderson disorder (see Appendix C). This indicates that our conclusion on the instability of QBCPs to TAI phases is robust to model details.

V. CONCLUSIONS

We studied a model of a QBC system under gap-opening and disorder-inducing couplings. A complete spectral, topological, and localization analysis was carried out in order to obtain a detailed phase diagram. We found not only that the topological phases existing in the clean limit were robust to disorder but also that new gapless topological phases were formed. Most importantly, we found a different instability of the QBCP: a disorder-induced instability to gapless topological phases with Chern numbers $C = \pm 1$ that are absent in the clean limit. The possibility of emulating quantum Hamiltonians using ultracold gases of atoms in an optical lattices [50,51] opens interesting prospects to realize the observed phases experimentally. In particular, the ability to realize disordered or quasiperiodic potentials in the system to induce localization phenomena was recently achieved [52,53].

An interesting question for future work is whether instabilities of the QBCPs to electron-electron interactions can give rise to topological phases with properties similar to the gapless topological insulators uncovered here. A full phase diagram capturing the interplay between disorder and interactions would then be a natural follow-up.

ACKNOWLEDGMENTS

N.S. and E.V.C. acknowledge partial support from Fundação para a Ciência e Tecnologia (FCT-Portugal) through Grant No. UIDB/04650/2020. M.G. acknowledges partial

support from Fundação para a Ciência e Tecnologia (FCT-Portugal) through Grant No. UID/CTM/04540/2019. M.G. acknowledges further support from FCT-Portugal through Grant No. SFRH/BD/145152/2019.

APPENDIX A: REAL-SPACE HAMILTONIAN

In this Appendix, we present the full real-space Hamiltonian, which can be divided in two contributions,

$$H_0 = H_{\mathrm{QBC}} + H_B,$$

where each term is given by

$$\begin{aligned} H_{\mathrm{QBC}} = {} & t\sum_{\boldsymbol{R}} a^\dagger_{\boldsymbol{R}} a_{\boldsymbol{R}+\boldsymbol{e}_x} - t\sum_{\boldsymbol{R}} a^\dagger_{\boldsymbol{R}} a_{\boldsymbol{R}+\boldsymbol{e}_y} + \mathrm{H.c.} \\ & - t\sum_{\boldsymbol{R}} b^\dagger_{\boldsymbol{R}} b_{\boldsymbol{R}+\boldsymbol{e}_x} + t\sum_{\boldsymbol{R}} b^\dagger_{\boldsymbol{R}} b_{\boldsymbol{R}+\boldsymbol{e}_y} + \mathrm{H.c.} \\ & + \frac{t}{2}\sum_{\boldsymbol{R}} a^\dagger_{\boldsymbol{R}} b_{\boldsymbol{R}+\boldsymbol{e}_x+\boldsymbol{e}_y} + \frac{t}{2}\sum_{\boldsymbol{R}} a^\dagger_{\boldsymbol{R}} b_{\boldsymbol{R}-\boldsymbol{e}_x-\boldsymbol{e}_y} + \mathrm{H.c.} \\ & - \frac{t}{2}\sum_{\boldsymbol{R}} a^\dagger_{\boldsymbol{R}} b_{\boldsymbol{R}+\boldsymbol{e}_x-\boldsymbol{e}_y} - \frac{t}{2}\sum_{\boldsymbol{R}} a^\dagger_{\boldsymbol{R}} b_{\boldsymbol{R}-\boldsymbol{e}_x+\boldsymbol{e}_y} + \mathrm{H.c.}, \end{aligned}$$

and

$$\begin{aligned} H_B = {} & i\sum_{\boldsymbol{R}} a^\dagger_{\boldsymbol{R}} b_{\boldsymbol{R}} + \mathrm{H.c.} \\ & + i\frac{B+1}{4}\sum_{\boldsymbol{R}} a^\dagger_{\boldsymbol{R}} b_{\boldsymbol{R}+\boldsymbol{e}_x} + i\frac{B+1}{4}\sum_{\boldsymbol{R}} a^\dagger_{\boldsymbol{R}} b_{\boldsymbol{R}-\boldsymbol{e}_x} + \mathrm{H.c.} \\ & + i\frac{B+1}{4}\sum_{\boldsymbol{R}} a^\dagger_{\boldsymbol{R}} b_{\boldsymbol{R}+\boldsymbol{e}_y} + i\frac{B+1}{4}\sum_{\boldsymbol{R}} a^\dagger_{\boldsymbol{R}} b_{\boldsymbol{R}-\boldsymbol{e}_y} + \mathrm{H.c.} \end{aligned}$$

Additionally, we present a schematic representation of this Hamiltonian in Fig. 6.

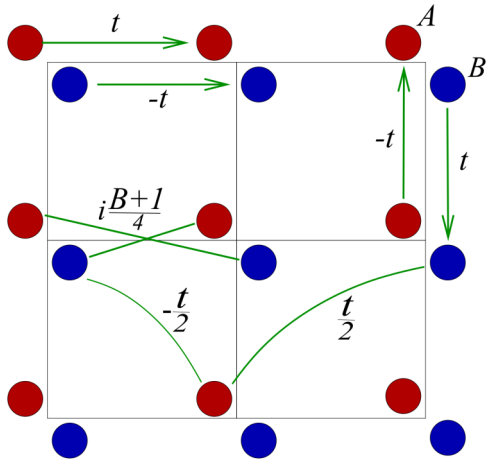

FIG. 6. Schematic representation of the tight-binding Hamiltonian. Red dots represent the A orbitals, while blue ones correspond to the B orbitals.

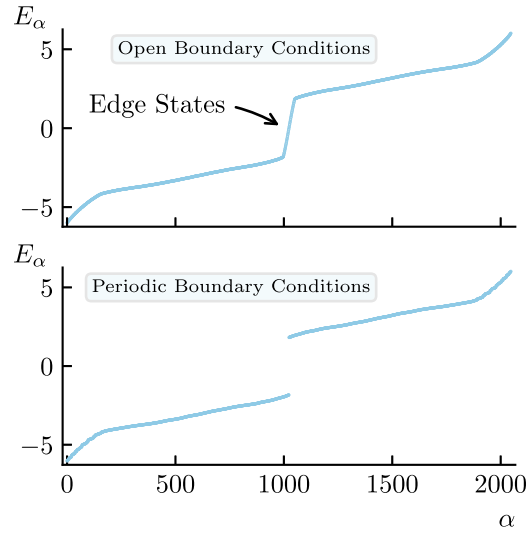

FIG. 7. Eigenenergies for $B = -1$ and $W = 1$ for a system size of $N = 32 \times 32$ for a single disorder configuration.

APPENDIX B: TOPOLOGICAL EDGE STATES AND OPEN BOUNDARY CONDITIONS

In this Appendix, we show results that further explore the topological phases. One consequence of nontrivial topology is the presence of edge states, with energies inside the gap, when considering open boundary conditions. For $B = -6$ and $W = 1$ (which puts the system in a $C = 2$ region), the system is gapped for periodic boundary conditions. Opening the boundaries, new states appear on the gap at all energies inside the gap, as can be seen in Fig. 7.

The states inside the gap, when considering open boundary conditions, are indeed edge states, as shown in Fig. 8, where we plot the probability density for a state inside the gap with energy $E = 0$.

For stronger disorder, the system is in a gapless region, where the open boundary conditions and periodic boundary conditions cannot be distinguished through the spectrum. Nonetheless, since the bulk eigenstates are localized and the edge states are delocalized over the edge, the latter can clearly be seen after disorder averaging is performed, as shown in Fig. 8.

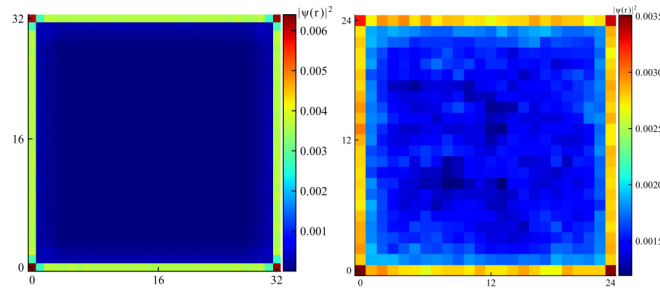

FIG. 8. Edges state probability density at the Fermi energy for $B = -6$ for two different disorder values. Left: $W = 1$ and 10 disorder configurations. Right: $W = 10$ and 1000 disorder configurations.

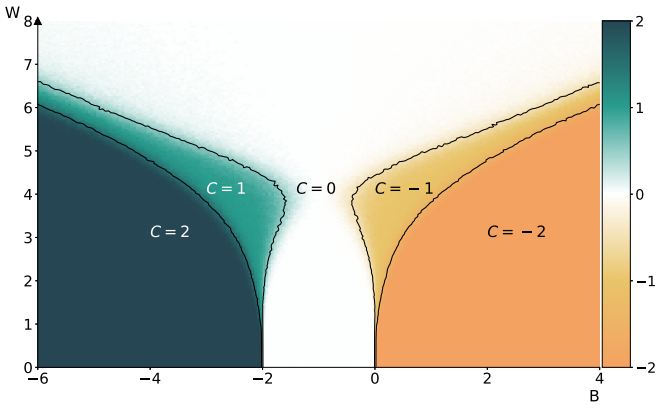

FIG. 9. Phase diagram with binary disorder. All points were averaged over 200 disorder configurations, and systems of size 15×15 were used.

APPENDIX C: QUALITATIVE PHASE DIAGRAM FOR BINARY DISORDER

In this Appendix, we present the phase diagram for binary disorder. In this case, the on-site potentials ϵ_i are randomly generated according to the following distribution:

$$P_V(\varepsilon_i) = \tfrac{1}{2}[\delta(\varepsilon_i) + \delta(V - \varepsilon_i)].$$

The Chern number results are shown in Fig. 9. Qualitatively, the phase diagram is very similar to the one obtained for Anderson disorder in Fig. 1. In particular, the disorder-induced $C = \pm 1$ topological phases are still present, and the reentrant TAI behavior is also observed. However, a smaller degree of disorder is needed to destroy all the nontrivial phases. In addition, for large B (absolute value), the $C = \pm 1$ phases are much narrower with binary disorder, which means that they are more robust to Anderson disorder.

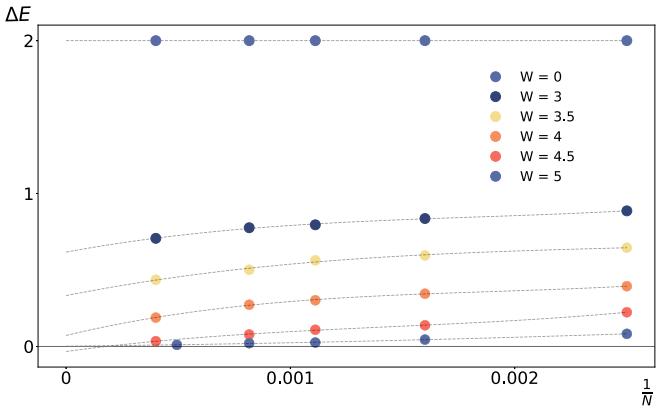

FIG. 10. Energy difference ΔE between the two states closest to the Fermi level, directly above and below, computed using exact diagonalization for systems with different disorder strengths W and varying numbers of sites N.

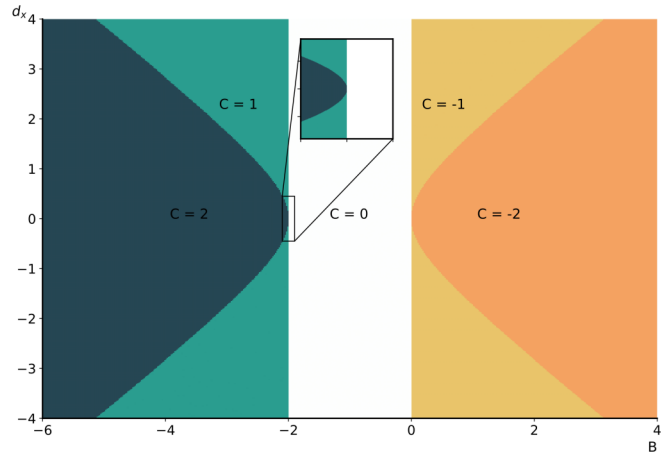

FIG. 11. Example of a perturbation that leads to a $C = 1$ phase without disorder.

APPENDIX D: GAPPED AND GAPLESS REGIONS

In this Appendix, we present the details of the criterion used in the main text to distinguish gapped and gapless regimes.

Due to the finite resolution of the KPM, it is typically challenging to find the transition point between gapped and gapless regimes. In particular, the DOS obtained with the KPM may have a finite spectral weight at energies within gaps if the system size and the number of polynomials are not large enough. We therefore use finite-size scaling results from exact diagonalization to find a suitable ρ_{cut} below which the KPM DOS should be considered null. For the system to be gapless, the energy difference ΔE between the two states closest to the Fermi level, immediately above and below, must converge to zero in the thermodynamic limit, $\Delta E \to 0$. To define ρ_{cut}, we set the parameter $B = -1$. Results for ΔE as a function of inverse system size $1/N$ are shown in Fig. 10. After fitting the finite-size scaling results to a cubic function and extrapolating to $N \to \infty$, we observe that for disorder around $W \approx 4.2$ the system must be gapless. It is then just a matter of computing

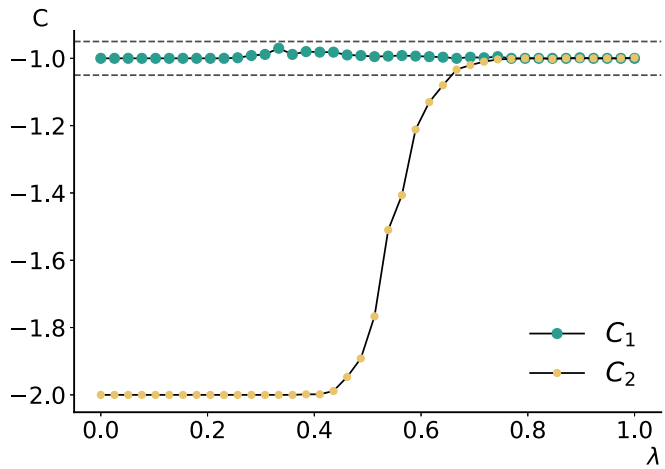

FIG. 12. Chern number computed along the paths $\mathcal{P}_1$ and $\mathcal{P}_2$ defined by Eqs. (E2) and (E3), respectively. All points were averaged over 600 disorder realizations for a system of size 45×45.

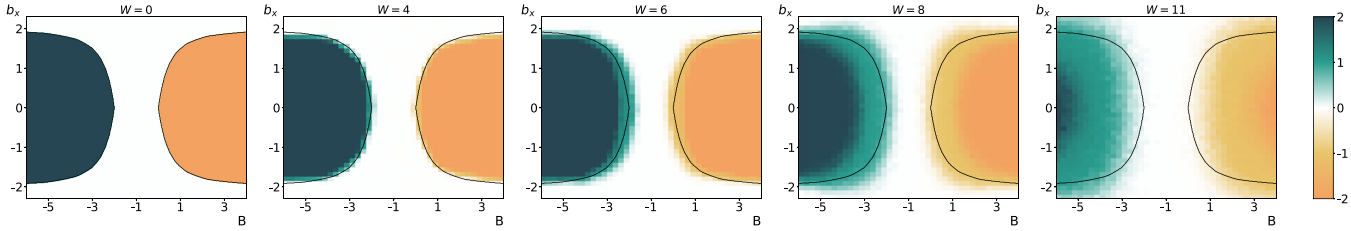

FIG. 13. Evolution of the phase diagram in the B-b_x plane. The black lines correspond to the phase transition for null disorder corresponding to the points where there are Dirac cones or QBCPs in the spectrum. All points were averaged with 100 disorder configurations for systems of size 15×15.

the DOS with KITE [34] for $B = -1$ with that critical disorder and then fixing $\rho(E = 0)$ obtained with KITE to be ρ_{cut}.

APPENDIX E: $|C| = 1$ TRANSLATIONAL INVARIANT PHASES

Here we provide an example of a possible $\mathbf{k}$-dependent translationally invariant perturbation that leads to a $C = 1$ phase:

$$\Sigma_x(\mathbf{k}) = d_x \sin(k_x + k_y). \tag{E1}$$

Results for the topological phases as a function of B and d_x are found in Fig. 11. To see that these phases are adiabatically connected to the $C = \pm 1$ disorder-induced phases we compute the Chern number in a parameter path $\mathcal{P}_1$ given by the pair (d_x, W):

$$\mathcal{P}_1 : (d_x, W) = \begin{cases} (0.7, 12\lambda), & 0 < \lambda \leqslant \frac{1}{2}, \\ (1.4(1-\lambda), 6), & \frac{1}{2} < \lambda \leqslant 1, \end{cases} \tag{E2}$$

where we have fixed B to $B = 0.1$. For $\lambda = 0$, the model has the self-energy given in Eq. (E1) and is in the $C = -1$ phase of the phase diagram shown in Fig. 11. When $\lambda = 1$, we have $d_x = 0$, which is a point of the phase diagram in Fig. 1 with $C = -1$. It can be seen in Fig. 12 that the system has $C = -1$ for all points along the $\mathcal{P}_1$ path. The $\mathcal{P}_2$ path, which is defined as

$$\mathcal{P}_2 : (d_x, W) = (0, 6\lambda), \quad 0 < \lambda \leqslant 1, \tag{E3}$$

shows that the $C = -2$ phase may then be reached by decreasing disorder ($\lambda = 1 \to 0$), in total agreement with the phase diagram in Fig. 1.

APPENDIX F: EVOLUTION OF THE PHASE DIAGRAM WITH b_x CONSTANT PERTURBATION

To study the robustness of the QBCP we introduce the term $\boldsymbol{b} \cdot \boldsymbol{\sigma}$ in the Hamiltonian written in reciprocal space, where $\boldsymbol{b}$ can be a constant vector with three components, $\boldsymbol{b} = (b_x, b_y, b_z)$. The b_x perturbation lifts the degeneracy of the QBCP, splitting it into two Dirac cones. In Fig. 13, we show the value of the Chern number in the plane $\boldsymbol{B}$ vs $\boldsymbol{b_x}$ with increasing disorder. For a small b_x the phase diagram in Fig. 2 is practically unchanged. It is also clear from Fig. 13 that the $C = \pm 1$ phases exist even when $b_x \neq 0$.

[1] M. Z. Hasan and C. L. Kane, Rev. Mod. Phys. **82**, 3045 (2010).
[2] X.-L. Qi and S.-C. Zhang, Rev. Mod. Phys. **83**, 1057 (2011).
[3] B. A. Bernevig and T. L. Hughes, *Topological Insulators and Topological Superconductors* (Princeton University Press, Princeton, NJ, 2013).
[4] C.-K. K. Chiu, J. C. Y. Teo, A. P. Schnyder, and S. Ryu, Rev. Mod. Phys. **88**, 035005 (2016).
[5] B. Wu, J. Song, J. Zhou, and H. Jiang, Chin. Phys. B **25**, 117311 (2016).
[6] A. Altland and M. R. Zirnbauer, Phys. Rev. B **55**, 1142 (1997).
[7] D. Xiao, M. C. Chang, and Q. Niu, Rev. Mod. Phys. **82**, 1959 (2010).
[8] B. Kramer and A. MacKinnon, Rep. Prog. Phys. **56**, 1469 (1993).
[9] M. Onoda and N. Nagaosa, Phys. Rev. Lett. **90**, 206601 (2003).
[10] M. Onoda, Y. Avishai, and N. Nagaosa, Phys. Rev. Lett. **98**, 076802 (2007).
[11] E. V. Castro, M. P. López-Sancho, and M. A. H. Vozmediano, Phys. Rev. B **92**, 085410 (2015).
[12] E. V. Castro, R. de Gail, M. P. López-Sancho, and M. A. H. Vozmediano, Phys. Rev. B **93**, 245414 (2016).
[13] T. Morimoto, A. Furusaki, and C. Mudry, Phys. Rev. B **91**, 235111 (2015).
[14] A. P. Schnyder, S. Ryu, A. Furusaki, and A. W. W. Ludwig, Phys. Rev. B **78**, 195125 (2008).
[15] K. Sun, H. Yao, E. Fradkin, and S. A. Kivelson, Phys. Rev. Lett. **103**, 046811 (2009).
[16] S. Uebelacker and C. Honerkamp, Phys. Rev. B **84**, 205122 (2011).
[17] J. M. Murray and O. Vafek, Phys. Rev. B **89**, 201110(R) (2014).
[18] S. Ray, M. Vojta, and L. Janssen, Phys. Rev. B **98**, 245128 (2018).
[19] T. S. Zeng, W. Zhu, and D. Sheng, npj Quantum Mater. **3**, 49 (2018).
[20] J. Wang, C. Ortix, J. van den Brink, and D. V. Efremov, Phys. Rev. B **96**, 201104(R) (2017).
[21] Y.-M. Dong, Y.-H. Zhai, D.-X. Zheng, and J. Wang, Phys. Rev. B **102**, 134204 (2020).
[22] J. Li, R.-L. Chu, J. K. Jain, and S.-Q. Shen, Phys. Rev. Lett. **102**, 136806 (2009).
[23] C. W. Groth, M. Wimmer, A. R. Akhmerov, J. Tworzydło, and C. W. J. Beenakker, Phys. Rev. Lett. **103**, 196805 (2009).
[24] C. L. Kane and E. J. Mele, Phys. Rev. Lett. **95**, 226801 (2005).

[25] C. P. Orth, T. Sekera, C. Bruder, and T. L. Schmidt, Sci. Rep. **6**, 24007 (2016).
[26] J. Song, H. Liu, H. Jiang, Q. F. Sun, and X. C. Xie, Phys. Rev. B **85**, 195125 (2012).
[27] J. H. García, L. Covaci, and T. G. Rappoport, Phys. Rev. Lett. **114**, 116602 (2015).
[28] M. Gonçalves, P. Ribeiro, and E. V. Castro, arXiv:1807.11247.
[29] S.-N. Liu, G.-Q. Zhang, L.-Z. Tang, and D.-W. Zhang, Phys. Lett. A **431**, 128004 (2022).
[30] L.-Z. Tang, S.-N. Liu, G.-Q. Zhang, and D.-W. Zhang, Phys. Rev. A **105**, 063327 (2022).
[31] T. S. Gonçalves, M. Gonçalves, P. Ribeiro, B. Amorim, and E. V. Castro, arXiv:2212.08024.
[32] D.-W. Zhang, L.-Z. Tang, L.-J. Lang, H. Yan, and S.-L. Zhu, Sci. China: Phys., Mech. Astron. **63**, 267062 (2020).
[33] F. D. M. Haldane, Phys. Rev. Lett. **61**, 2015 (1988).
[34] S. M. João, M. Andelković, L. Covaci, T. G. Rappoport, J. M. V. P. Lopes, and A. Ferreira, R. Soc. Open Sci. **7**, 191809 (2020).
[35] T. Fukui, Y. Hatsugai, and H. Suzuki, J. Phys. Soc. Jpn. **74**, 1674 (2005).
[36] Y. F. Zhang, Y. Y. Yang, Y. Ju, L. Sheng, R. Shen, D. N. Sheng, and D. Y. Xing, Chin. Phys. B **22**, 11 (2013).
[37] A. MacKinnon and B. Kramer, Phys. Rev. Lett. **47**, 1546 (1981).
[38] A. MacKinnon and B. Kramer, Z. Phys. B **53**, 1 (1983).
[39] K. Hoffmann and M. Schreiber, *Computational Physics: Selected Methods Simple Exercises Serious Applications* (Springer, Berlin, 2012).
[40] G.-G. Liu, Y. Yang, X. Ren, H. Xue, X. Lin, Y.-H. Hu, H.-X. Sun, B. Peng, P. Zhou, Y. Chong, and B. Zhang, Phys. Rev. Lett. **125**, 133603 (2020).
[41] S. Stützer, Y. Plotnik, Y. Lumer, P. Titum, N. H. Lindner, M. Segev, M. C. Rechtsman, and A. Szameit, Nature (London) **560**, 461 (2018).
[42] J. Song, Y.-Y. Zhang, Y. Li, and Q. Sun, J. Phys.: Condens. Matter **27**, 045601 (2015).
[43] Y. Su, Y. Avishai, and X. R. Wang, Phys. Rev. B **93**, 214206 (2016).
[44] Y. Kuno, Phys. Rev. B **100**, 054108 (2019).
[45] H.-C. Hsu and T.-W. Chen, Phys. Rev. B **102**, 205425 (2020).
[46] H.-B. Wu and J.-J. Liu, Phys. Rev. B **103**, 115430 (2021).
[47] Y. Hatsugai, K. Ishibashi, and Y. Morita, Phys. Rev. Lett. **83**, 2246 (1999).
[48] Z.-G. Song, Y.-Y. Zhang, J.-T. Song, and S.-S. Li, Sci. Rep. **6**, 19018 (2016).
[49] Y.-B. Yang, K. Li, L.-M. Duan, and Y. Xu, Phys. Rev. B **103**, 085408 (2021).
[50] M. Lewenstein, A. Sanpera, V. Ahufinger, B. Damski, A. Sen(De), and U. Sen, Adv. Phys. **56**, 243 (2007).
[51] I. Bloch, J. Dalibard, and W. Zwerger, Rev. Mod. Phys. **80**, 885 (2008).
[52] M. Schreiber, S. S. Hodgman, P. Bordia, H. P. Lüschen, M. H. Fischer, R. Vosk, E. Altman, U. Schneider, and I. Bloch, Science **349**, 842 (2015).
[53] J.-Y. Choi, S. Hild, J. Zeiher, P. Schauß, A. Rubio-Abadal, T. Yefsah, V. Khemani, D. A. Huse, I. Bloch, and C. Gross, Science **352**, 1547 (2016).